CHAPTER VI
RESULTS AND DISCUSSION

4.1 Feed Biodiesel Analysis

In order to determine FAME composition of the feed biodiesel, a gas chromatograph (GC) equipped with a flame ionization detector (FID) was applied. The FAME compositions of feed biodiesel are shown in Table 4.1. In addition, a GC chromatogram of the overall FAME composition of feed biodiesel is presented in Figure 4.1.

Biodiesel compositions are mainly *cis*-methyl oleate (24.81%), methyl linoleate (50.93%), methyl linolenate (4.86%), methyl stearate (3.62%) and methyl palmitate (12.04%). The five most important fatty acid (C16:1, C18:0, C18:1, C18:2, C18:3) in weight percentage accounted for almost 96% of total fatty acid. On the other hand, a high content of fully saturated compounds has a very negative impact on the cold properties of the fuel (cloud point and pour point). So the decreases of polyunsaturates such as methyl stearate (C18:3) and methyl linoleate (C18:2) and the increase of *cis*-methyl oleate (*cis*-C18:1) will improve the properties of biodiesel (Yang *et al.*, 2010). For the biodiesel feedstock, soybean oil was selected due to its high unsaturated compositions as compared to other vegetable oils such as rapeseed or palm oil (Hoekman *et al.*, 2012).

Figure 4.2 shows an FT-IR spectrum of feed biodiesel. The peak at 3006 cm^{-1} corresponding to =C-H stretching in *cis*-configuration indicates the presence of unsaturated FAMEs, where nearly all of the double bonds in the feed biodiesel are in the *cis*-form. The peaks at 1742 cm^{-1} and 1169 cm^{-1}, which corresponds to C=O stretching and (C=O)-O stretching of FAME were also detected, respectively (Numwong *et al.*, 2012).

Table 4.1 FAME composition of feed biodiesel

| FAME	Structure	%
methyl myristate	C14:0	0.12
methyl palmitate	C16:0	12.04
methyl palmitelaidate	*trans*-C16:1	0.11
methyl palmitoleate	*cis*-C16:1	0.02
methyl heptadecanoate	C17:0	0.40
methyl stearate	C18:0	3.62
trans-methyl elaidate	*trans*-C18:1	0.14
cis-methyl oleate	*cis*-C18:1	24.81
methyl linoleate	C18:2	50.93
methyl linolenate	C18:3	4.86
methyl arachidate	C20:0	0.97
methyl *trans*-eicosenoate	*trans*-C20:1	0.17
methyl *cis*-eicosenoate	*cis*-C20:1	0.06
methyl behenate	C22:0	0.36
methyl lignocerate	C24:0	0.17
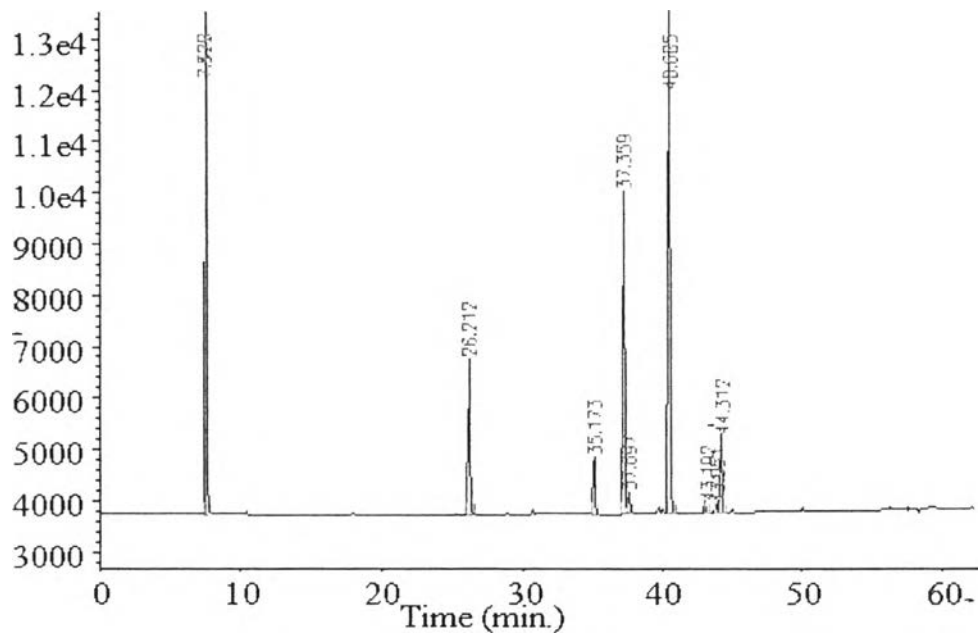
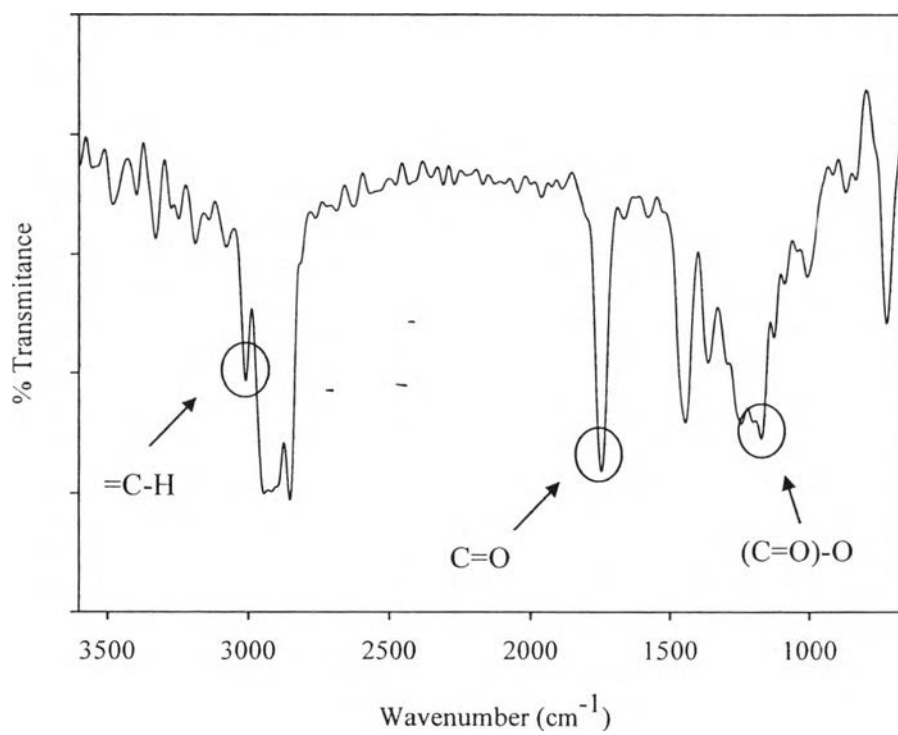**Figure 4.1** Chromatogram of feed biodiesel obtain from gas chromatograph.

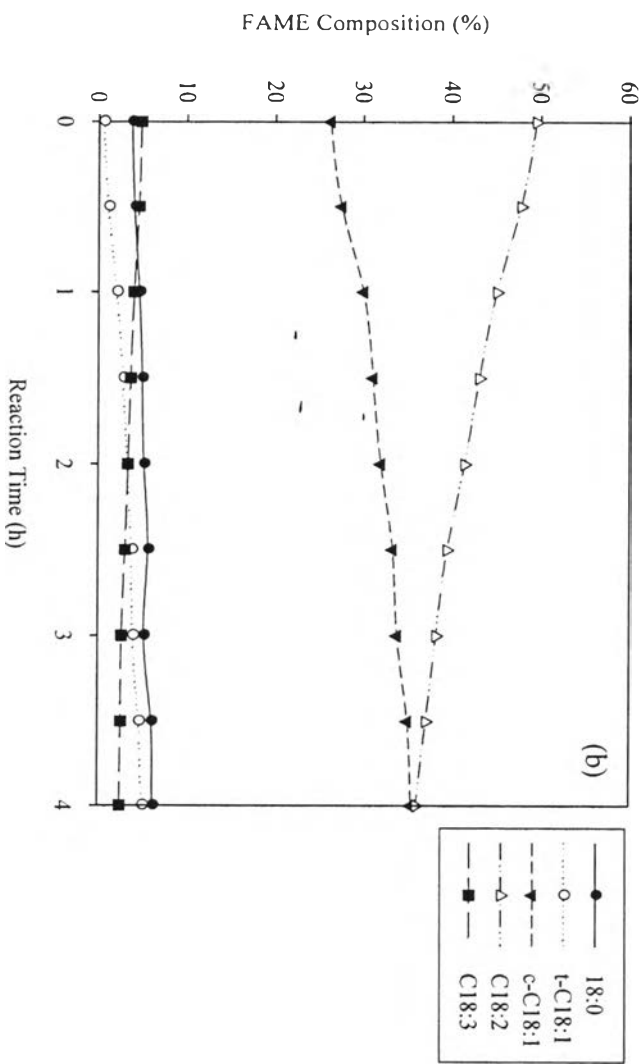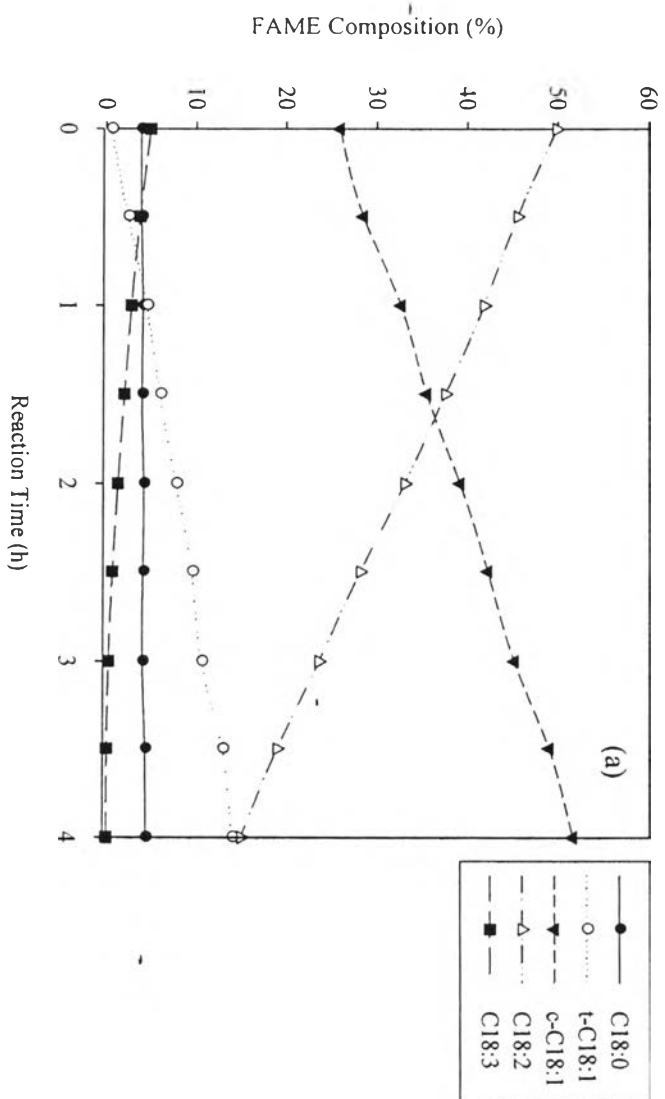**Figure 4.2** FTIR spectrum of feed biodiesel.

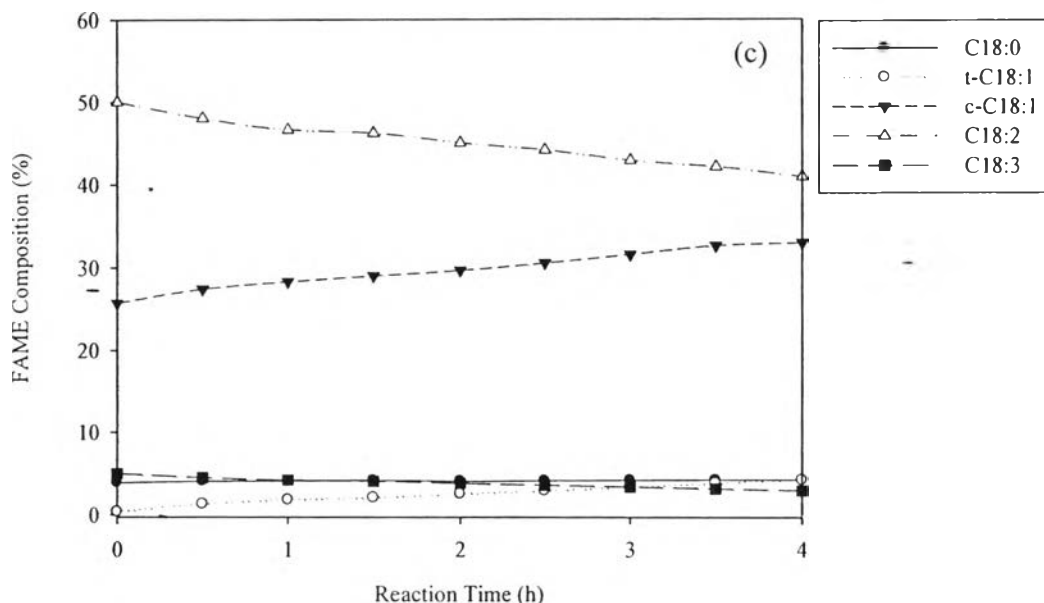## 4.2 Effect of Reaction Temperature on Partial Hydrogenation

To study the effect of reaction temperature on partial hydrogenation of soybean oil-based biodiesel, the reaction was carried out on three types catalysts; Pd/SiO_2, Pt/SiO_2, and Ni/SiO_2. The temperature was varied from 80 °C to 100 °C and 120 °C, respectively. The operating conditions were operated at 4 bar of hydrogen partial pressure, 150 ml/min of hydrogen flow rate, 1000 rpm of stirring rate, and 1 wt.% of the catalyst compared to 130.395 g of feed biodiesel (150 ml).

For the partial hydrogenation reaction, the FAMEs composition of each catalyst; Pd/SiO_2, Pt/SiO_2, and Ni/SiO_2 consist of C14:0, C16:0, *trans*-C16:1, *cis*-C16:1, C17:1, C:20:0, *trans*-C20:1, *cis*-C20:1, C22:0, and C24:0 relatively kept constant along the reaction time. The FAME compositions of catalysts are shown in Table 4.2. Therefore, all C18 compositions would be mainly focused in this study. The percentages of C18:0, *cis*-C18:1, *trans*-C18:1, C18:2, and C18:3 after partial hydrogenation reaction are shown in Figure 4.3.

Table 4.2 FAME compositions of catalysts after 4 h of reaction time (120 °C)

FAME	Structure	Compositions of FAME (%)		
		Pd/SiO$_2$	Pt/SiO$_2$	Ni/SiO$_2$
methyl myristate	C14:0	0.11	0.13	0.10
methyl palmitate	C16:0	12.55	11.63	11.66
methyl palmitelaidate	trans-C16:1	0.12	-	-
methyl palmitoleate	cis-C16:1	-	0.09	0.11
methyl heptadecanoate	C17:0	0.11	0.11	0.11
methyl stearate	C18:0	4.44	6.25	4.21
trans-methyl elaidate	trans-C18:1	14.02	5.06	4.23
cis-methyl oleate	cis-C18:1	51.58	35.48	32.96
methyl linoleate	C18:2	15.03	36.05	40.92
methyl linolenate	C18:3	0.10	2.52	2.92
methyl arachidate	C20:0	0.49	0.69	0.76
methyl trans-eicosenoate	trans-C20:1	-	0.29	0.24
methyl cis-eicosenoate	cis-C20:1	0.18	0.10	0.03
methyl behenate	C22:0	0.25	0.40	0.38
methyl lignocerate	C24:0	0.10	0.13	0.14

FAME Composition (%)

Reaction Time (h)

(a)

C18:0
t-C18:1
c-C18:1
C18:2
C18:3

FAME Composition (%)
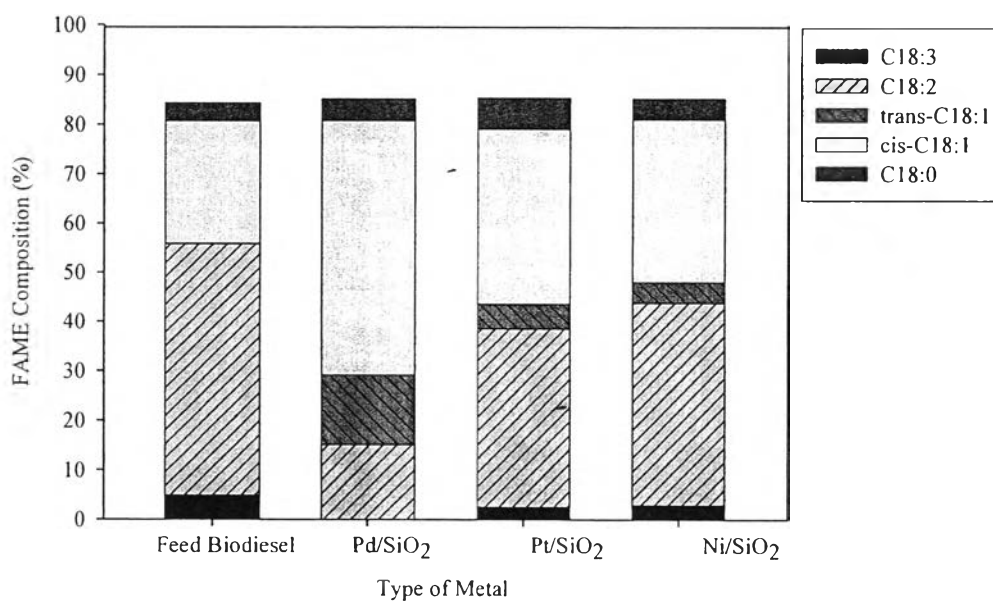
Reaction Time (h)

(b)

18:0
t-C18:1
c-C18:1
C18:2
C18:3

Figure 4.3 Effect of metal type: (a) 1 wt.% Pd/SiO₂ (b) 1.82 wt.% Pt/SiO₂ (c) 10 wt.% Ni/SiO₂ on FAME composition of biodiesel after partial hydrogenation reaction using catalyst reduced under H_2 at 300 °C (for Pd/SiO₂ and Pt/SiO₂) and 400 °C (for Ni/SiO₂) (Reaction condition: 120 °C, 4 bar, 150 ml/min of H_2 flow rate, 1000 rpm of stirring rate, and 1 wt.% of catalysts compared with 130.395 g of biodiesel).

The FAMEs composition after partial hydrogenation reaction using Pd/SiO₂ as a catalyst is shown in Figure 4.3(a). It showed that C18:3 gradually decreased from 4.91% to 0.10% and C18:2 rapidly decreased from 49.84% to 15.03%. C18:0 slightly increased from 3.88% to 4.44% within 4 h of the reaction. The composition of *trans*-C18:1 rapidly increased from 0.55% at initial and reached 14.02% after 4 h of the reaction, whereas the composition of *cis*-C18:1 rapidly increased from 25.94% to 51.58% after 4 h of the reaction. For the activity of Pt/SiO₂, the FAMEs composition is shown in Figure 4.3(b); C18:3 slowly decreased from 4.85% to 2.52% and C18:2 decreased from 49.45% to 36.05% after 4 h of the reaction time, whereas *cis*-C18:1 slightly increased from 26.24% to 35.48%. Interestingly, the composition of *trans*-C18:1 increased 0.54% to 5.06% within 4 h of reaction. The significant differences were found: Pd catalyst promoted the formation of *cis*-C18:1 faster than
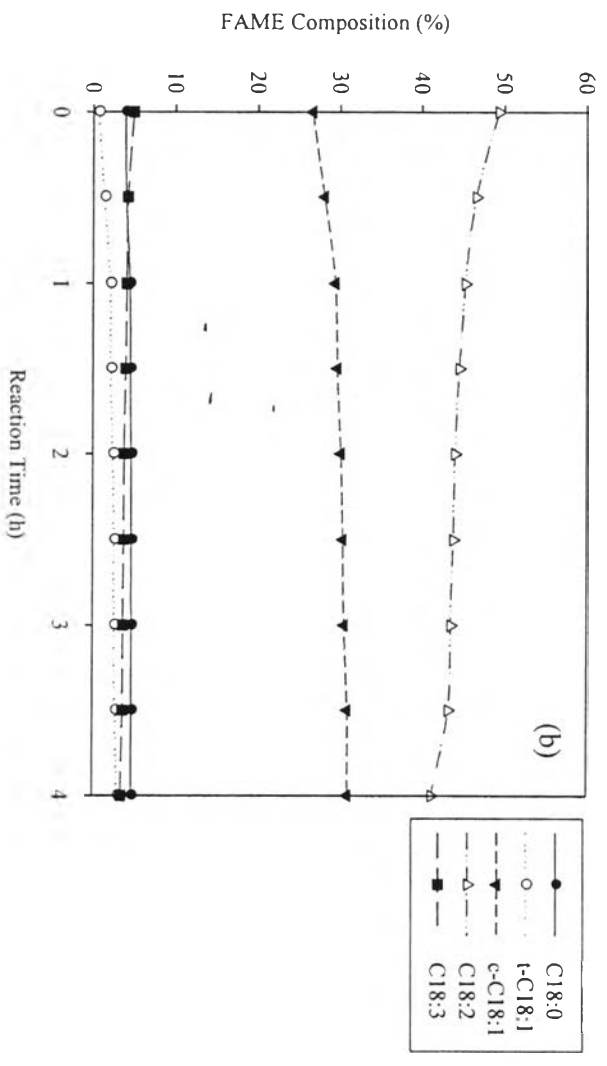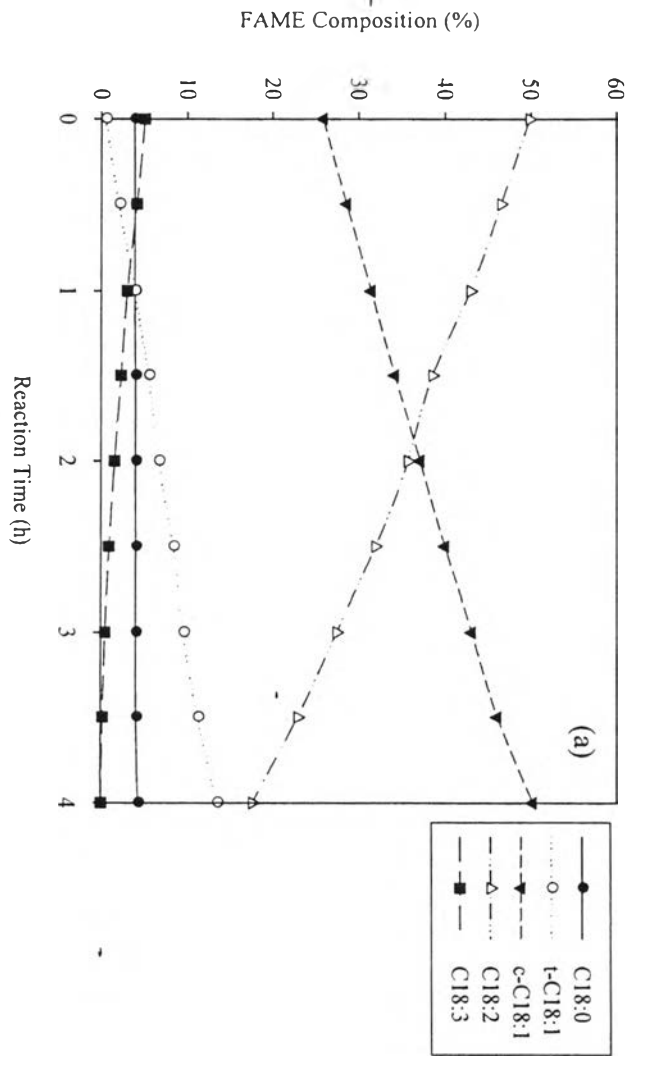
Pt catalyst. Composition of C18:0 gradually increased from 3.81% to 6.25% until the end of reaction. And the last, partial hydrogenation reaction by using Ni/SiO_2 as a catalyst, the FAMEs composition is shown in Figure 4.3(c); C18:3 and C18:2 decreased from 4.96% to 2.92% and 50.01% to 40.92%, respectively. While *cis*-C18:1 slightly increased from 25.74% to 32.96%. The *trans*-C18:1 content slightly increased from 0.37% to final values at 4.23% after 4 h of reaction.
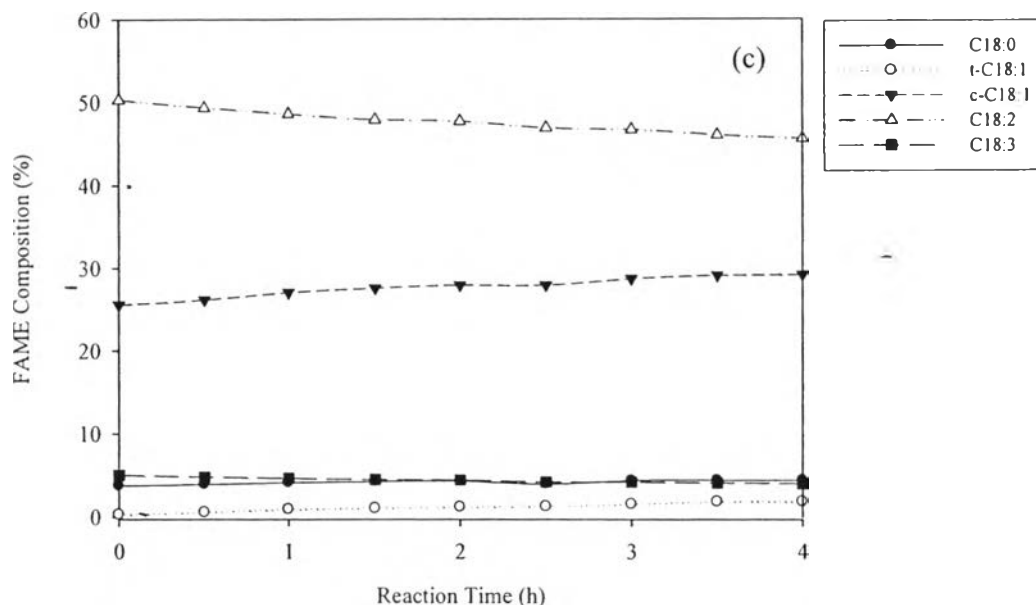
The results in Figure 4.4, evidently showed that the Pd catalyst presented the highest catalyst activity. Since, it could convert both C18:3 and C18:2 rapidly within 4 h of reaction time, and also increased the amount of *cis*-C18:1. For Pt and Ni catalysts, they followed the concept of partial hydrogenation. However, Ni catalyst showed the lowest catalytic activity. This result is consistent with the work done by Thunyaratchatanon 2012.

Figure 4.4 Comparison of C18 FAME composition of biodiesel after hydrogenation reaction (4 h) in conditions : 120 °C, 4 bar, 150 ml/min of H_2 flow rate, 1000 rpm of stirring rate, 1 wt.% of Palladium loading, 1.82 wt.% of Platinum loading, 10 wt.% of Ni loading, and 1 wt.% of catalyst.
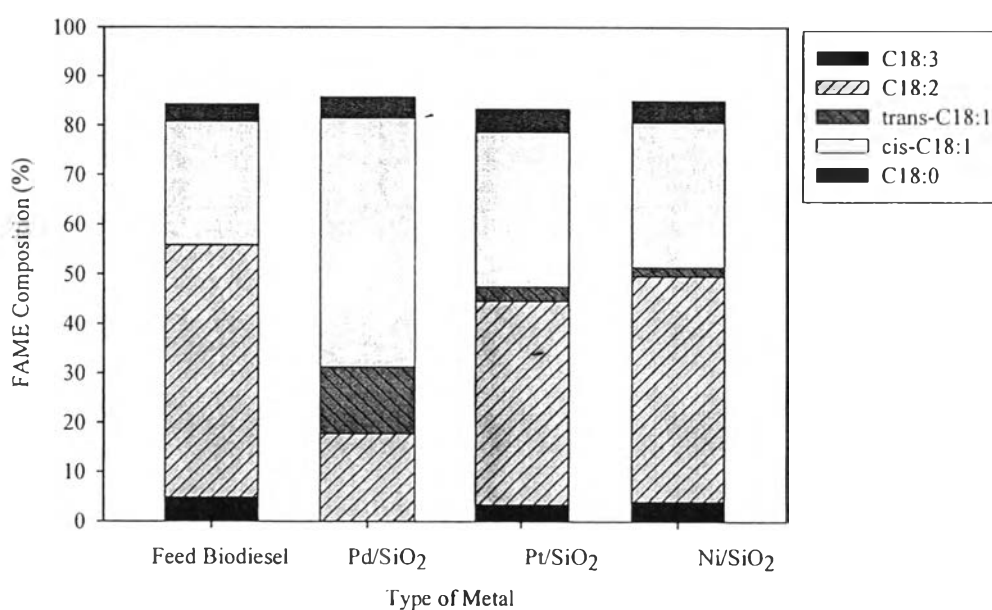
FAME Composition (%)

Reaction Time (h)

C18:0
t-C18:1
c-C18:1
C18:2
C18:3

(a)

FAME Composition (%)

Reaction Time (h)

C18:0
t-C18:1
c-C18:1
C18:2
C18:3

(b)

Figure 4.5 Effect of metal type: (a) 1 wt.% Pd/SiO$_2$ (b) 1.82 wt.% Pt/SiO$_2$ (c) 10 wt.% Ni/SiO$_2$ on FAME composition of biodiesel after partial hydrogenation reaction using catalyst reduced under H$_2$ at 300 °C (for Pd/SiO$_2$ and Pt/SiO$_2$) and 400 °C (for Ni/SiO$_2$) (Reaction condition: 100 °C, 4 bar, 150 ml/min of H$_2$ flow rate, 1000 rpm of stirring rate, and 1 wt.% of catalysts compared with 130.395 g of biodiesel).

For Pd/SiO$_2$, the FAMEs composition carried out at 100 °C are shown in Figure 4.5(a). It showed that C18:3 and C18:2 decreased from 5.03% to 0.05% and 49.84% to 17.65%, respectively, at 4 h of the reaction time. While C18:0 gradually increased from 3.83% to 4.33% after 4 h of the reaction. The cis-C18:1 content slightly increased from 25.91% to 50.22%. In addition, the trans-C18:1 content slightly increased from 0.50% to final values at 13.52% after 4 h of reaction. Catalytic activity of Pt/SiO$_2$ at 100 °C, the FAMEs composition is shown in Figure 4.5(b). It illustrated that C18:3 decreased from 4.91% to 3.43 and C18:2 slowly decreased from 49.30% to 41.21%. While C18:0 slightly increased from 3.88% at starting time to 4.72% at the end of reaction time. The content of cis-C18:1 gradually increased from 26.58% to 30.95% after 4 h of the reaction. The trans-C18:1 content

continually increased from 0.64% to 3.00% at 4 h of the reaction. And the partial hydrogenation reaction by using Ni/SiO_2 as a catalyst, it was operated at 100 °C, the FAMEs composition is shown in Figure 4.5(c). The composition of C18:3 and C18:2 slowly decreased from 5.04% to 4.00% and 50.26% to 45.56%, respectively. While *cis*-C18:1 slightly increased from 25.56% to 29.16%. The *trans*-C18:1 content slightly increased from 0.26% to final values at 1.86% after 4 h of reaction.

The catalytic activity of each catalyst is compared in Figure 4.6, the Pd catalyst presented the highest catalytic activity. Since, it could convert both C18:3 and C18:2 rapidly within 4 h of reaction time, and also increased the amount of *cis*-C18:1. For Pt and Ni catalysts, they followed the concept of partial hydrogenation. However, Ni catalyst showed the lowest catalytic activity. This result is consistent with the work done by Thunyaratchatanon 2012.

Figure 4.6 Comparison of C18 FAME composition of biodiesel after hydrogenation reaction (4 h) in conditions : 100 °C, 4 bar, 150 ml/min of H_2 flow rate, 1000 rpm of stirring rate, 1 wt.% of Palladium loading , 1.82 wt.% of Platinum loading, 10 wt.% of Ni loading, and 1 wt.% of catalyst.
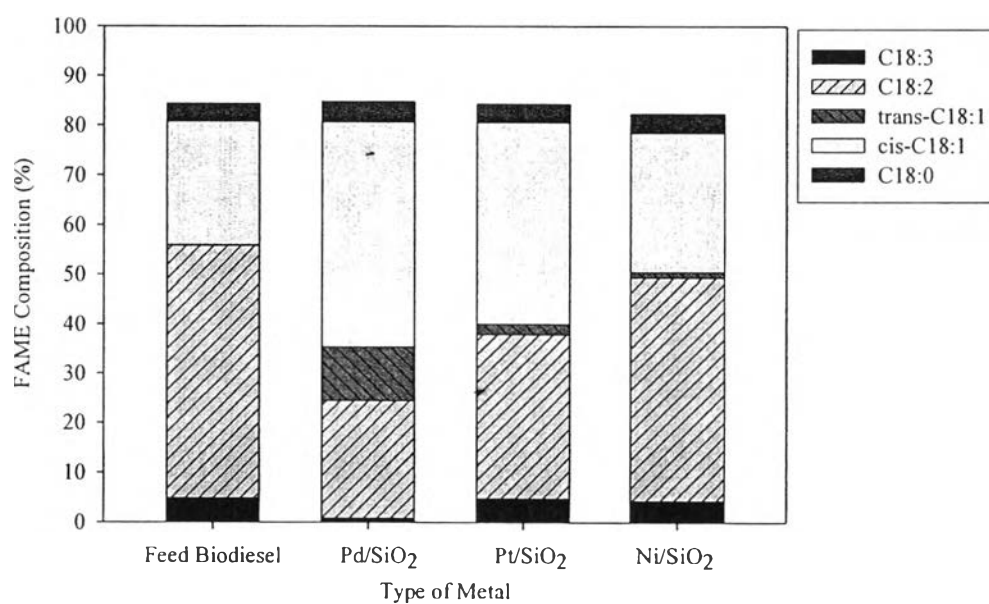
FAME Composition (%)

Reaction Time (h)

(a)

C18:0
t-C18:1
c-C18:1
C18:2
C18:3

(b)

C18:0
t-C18:1
c-C18:1
C18:2
C18:3
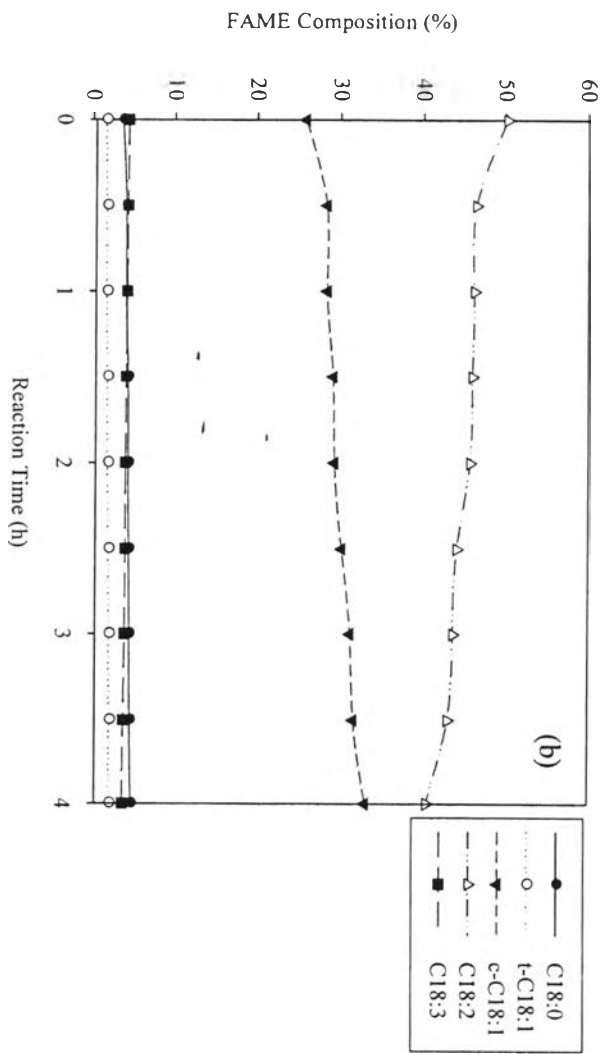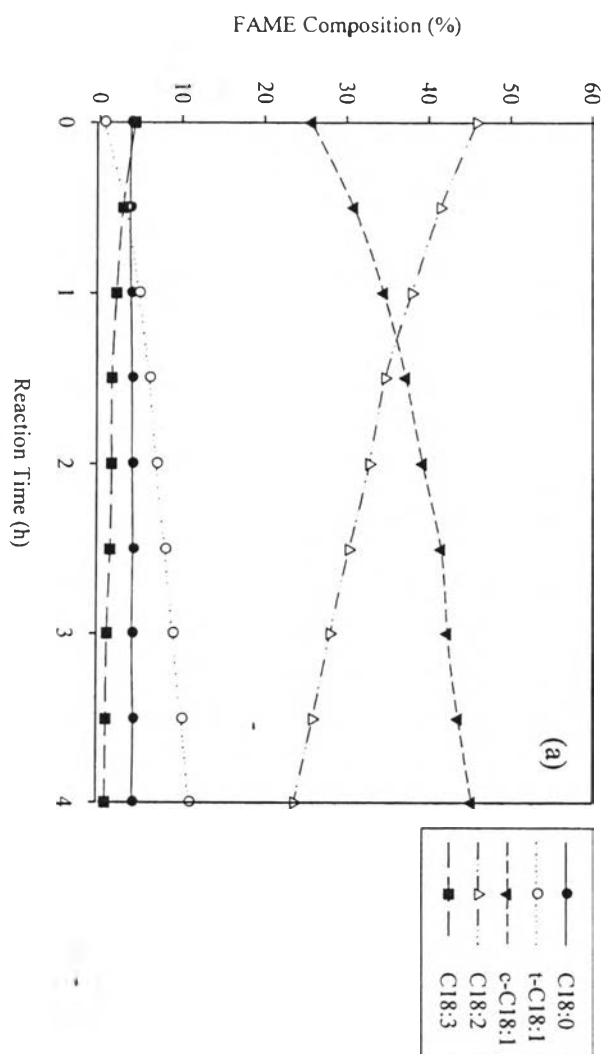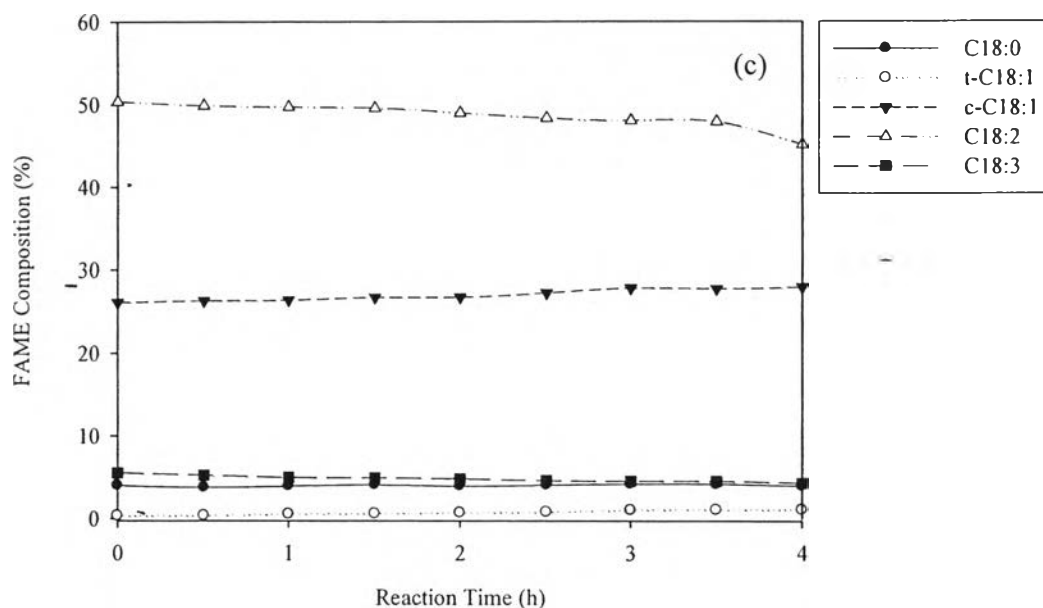
Figure 4.7 Effect of metal type: (a) 1 wt.% Pd/SiO₂ (b) 1.82 wt.% Pt/SiO₂ (c) 10 wt.% Ni/SiO₂ on FAME composition of biodiesel after partial hydrogenation reaction using catalyst reduced under H_2 at 300 °C (for Pd/SiO₂ and Pt/SiO₂) and 400 °C (for Ni/SiO₂) (Reaction condition: 80 °C, 4 bar, 150 ml/min of H_2 flow rate, 1000 rpm of stirring rate, and 1 wt.% of catalysts compared with 130.395 g of biodiesel).

At temperature of 80 °C, the catalytic activity of Pd/SiO₂ was studied, as shown in Figure 4.7(a). It exhibited that C18:3 and C18:2 dramatically decreased from 4.31% to 0.78% and 45.82% to 23.65%, respectively, after 4 h of the reaction. The level of C18:0 slightly increased from 3.84% to 4.11% after 4 h of reaction. For *cis*-C18:1 and *trans*-C18:1 increased from 25.70% to 45.26% and 0.56% to 10.95% at 4 h of the reaction time. For Pt/SiO₂ catalyst, the FAMEs composition carried out at 80 °C are shown in Figure 4.7(b). It showed that both C18:3 and C18:2 gradually decreased from 4.31% to 3.75% and 50.51% to 40.48%, respectively. Whereas the level of C18:0 continually increased from 3.57% to 4.80% at 4 h of the reaction time. In addition, the composition of both *cis*-C18:1 and *trans*-C18:1 gradually increased from 25.80% to 33.15% and 1.53% to 2.13%, respectively. And the last partial hydrogenation reaction by using Ni/SiO₂ as a catalyst, the FAMEs composition

carried out at 80 °C are shown in Figure 4.7(c). It exhibited that C18:3 and C18:2 decreased from 5.51% to 4.29% and 50.36% to 45.14%, respectively, at 4 h of the time reaction. The level of C18:0 slightly increased from 3.99% to 4.14% at 4 h of the reaction time. Both cis-C18:1 and trans-C18:1 gradually increased from 26.09% to 27.92% and 0.34% to 1.08%, respectively, after 4 h of the reaction.

The performance of each catalyst shown in Figure 4.8, evidently showed that the Pd catalyst presented the highest catalyst activity. Since, it could convert both C18:3 and C18:2 rapidly within 4 h of reaction time, and also increased the amount of cis-C18:1. For Pt and Ni catalysts, they followed the concept of partial hydrogenation. However, Ni catalyst showed the lowest catalytic activity. This result is consistent with the work done by Thunyaratchatanon 2012.

Figure 4.8 Comparison of C18 FAME composition of biodiesel after hydrogenation reaction (4 h) in conditions : 80 °C, 4 bar, 150 ml/min of H_2 flow rate, 1000 rpm of stirring rate, 1 wt.% of Palladium loading, 1.82 wt.% of Platinum loading, 10 wt.% of Ni loading, and 1 wt.% of catalyst.

From bar chart shown in Figure 4.9, it can be concluded that an increase in reaction temperature of partial hydrogenation of polyunsaturated FAMEs leads to an increase in *trans*-C18:1 content. This result is in accordance with the work done by Numwong and co-workers. They found that the increase in temperature caused an increase of *trans*-C18:1 and C18:0. This was a double bond migration and isomerization of the *cis*-C18:1 to the *trans*-C18:1 as the result of the higher temperature and higher reaction rate at the higher temperature according to kinetics principle (Numwong *et al.*, 2012). Interestingly, the Ni catalyst was carried out at 80 °C showed the lowest amount of *trans*-C18:1, *cis*-C18:1, and C18:0, and also showed the highest level of C18:2.
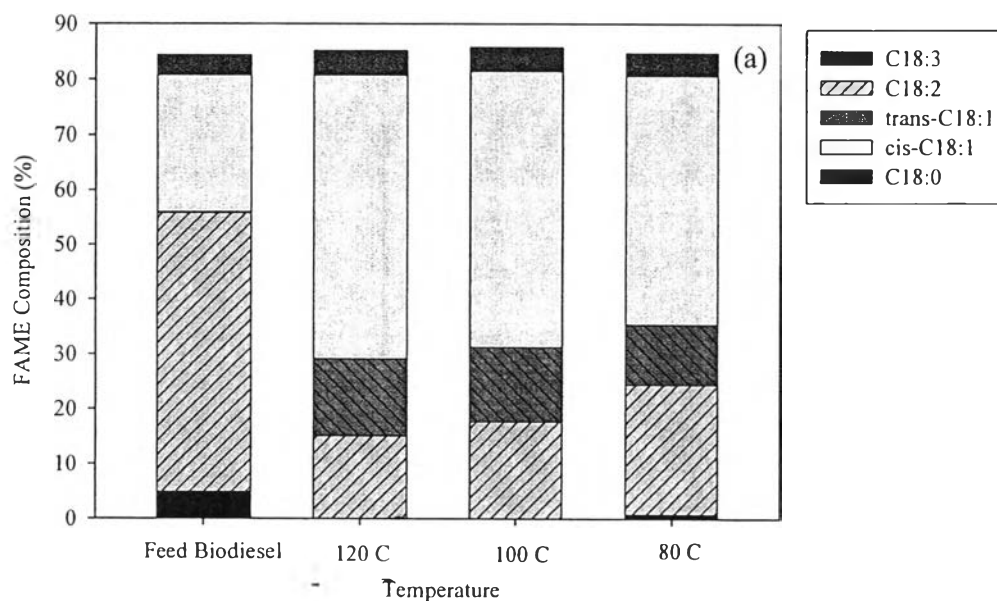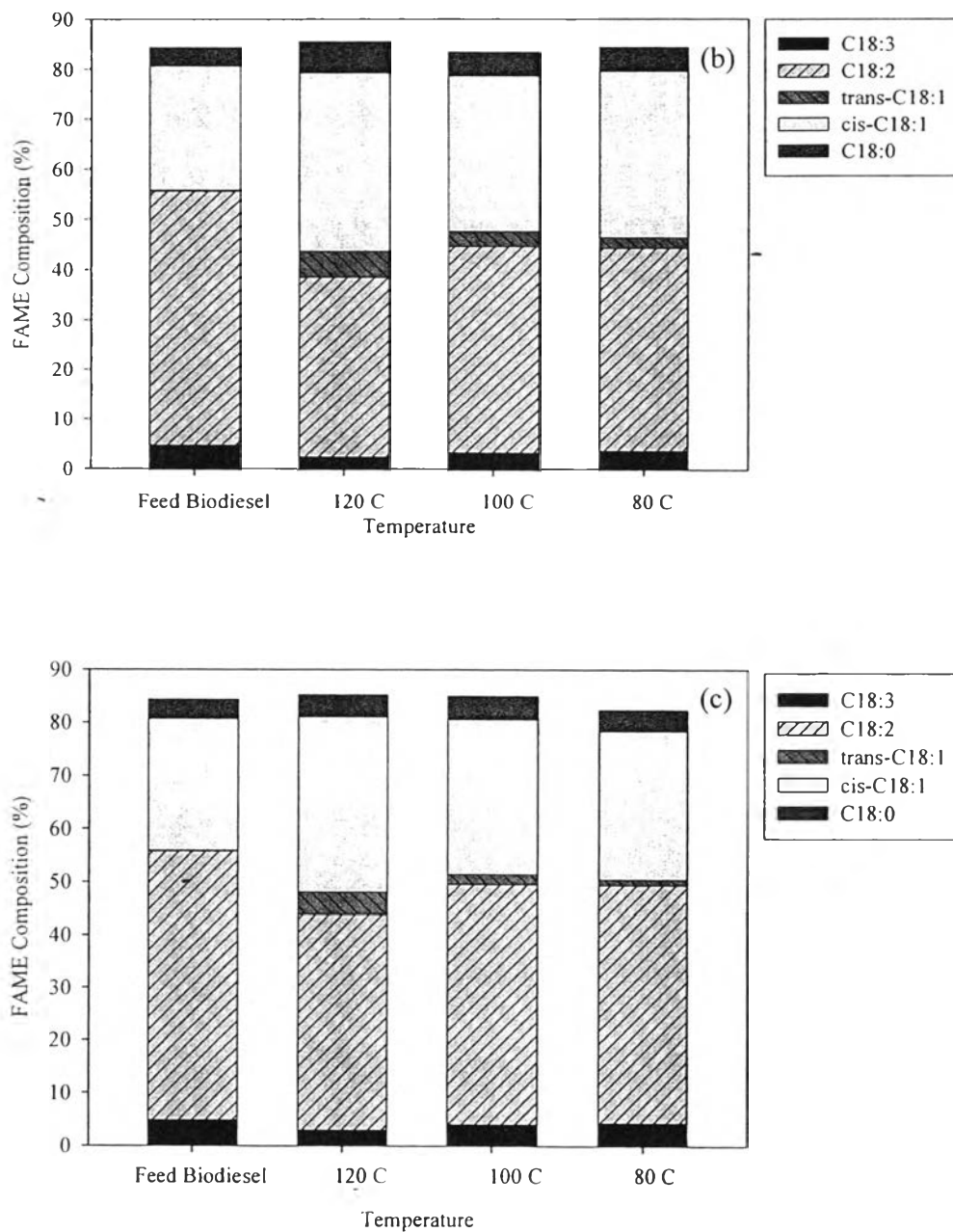
Figure 4.9 Effect of temperature: (a) 1 wt.% Pd/SiO₂ (b) 1.82 wt.% Pt/SiO₂ (c) 10 wt.% Ni/SiO₂ on FAME composition of biodiesel after partial hydrogenation reaction using catalyst reduced under H₂ at 300 °C (for Pd/SiO₂ and Pt/SiO₂) and 400 °C (for Ni/SiO₂) (Reaction condition: 120 °C-80 °C, 4 bar, 150 ml/min of H₂ flow rate, 1000 rpm of stirring rate, and 1 wt.% of catalysts compared with 130.395 g of biodiesel).

The actual metal content was determined by atomic absorption spectroscopy (AAS). These catalysts; Pd/SiO_2, Pt/SiO_2, and Ni/SiO_2 were prepared by incipient wetness impregnation (IWI) method using $Pd(NH_3)_4.Cl_2$, $Pt(NH_3)_4.Cl_2.H_2O$, and $Ni(NO_3)_2.6H_2O$ precursors, respectively. The percentages of metal loading on each type of catalysts determined by AAS are shown in Table 4.3. In this work, 1 wt.% Pd was loaded on Pd/SiO_2, the actual metal contents were about 0.93 wt.%. For 1.82 wt.% of Pt catalyst loaded on Pt/SiO_2, the actual amounts of Pt were about 1.62 wt.%. Using Ni as catalyst, the metal was loaded 10 wt.% on Ni, the actual Ni contents were about 9.46 wt.%.

Table 4.3 The percentage of metal loading on each type of catalysts

Catalysts	Metal loading (wt.%)	
	Expected Loading	Actual Loading
Pd/SiO_2	1.0	0.93
Pt/SiO_2	1.82	1.62
Ni/SiO_2	10.0	9.46

The catalytic activities of the prepared catalysts used in partial hydrogenation of biodiesel are shown by turnover frequency (TOF) which calculated from C18:2 conversion within 4 h of reaction time. TOF was applied in order to confirm the catalytic activity of each catalyst. The turnover frequency equation is shown below;

$$TOF\ (h^{-1}) = \left[\frac{\frac{\%conversion}{100} \times Amount\ of\ biodiesel\ (g)}{\frac{wt.\%metal}{100} \times \frac{\%metal\ dispersion}{100} \times W_{catalyst}(g)} \right] \div time$$

Where

% conversion = $C18:2_{t=0hr} - C18:2_{t=4hr}$

Amount of biodiesel = 130.395 g

$W_{catalyst}$ = 1.30395 g (1 wt.% catalyst compared to amount of biodiesel (g))

Time = 4 h

The activity of the catalysts in term of TOF is displayed in Table 4.4. The order of the activity of each catalyst based on TOF was: Ni catalyst < Pt catalyst < Pd catalyst. This can be explained that Pd catalyst could be the most active catalyst. It suddenly converted C18:2 within 4 h of reaction time and followed by Pt and Ni catalyst, respectively. These results were consistent with Thunyaratchatanon 2012. Moreover, this study also agrees well with MaAdel *et al.*, 2011. They found that Pd based catalysts are the most active compared to the Ni catalyst and the Pt catalyst for oil hydrogenation.

The percentages of metal dispersion of each catalyst measured by a CO pulse adsorption method are displayed in Table 4.4. The metal dispersion of Pd, Pt, and Ni were about 14.0%, 7.42%, and 5.60%, respectively. It is noticed that Pd dispersion has the highest value which indicated that Pd metals well dispersed on silica support. While Ni has the lowest dispersion value. The order of the particle size of each catalysts were: Pd (1 wt.% metal loading) > Pt (1.82 wt.% metal loading) > Ni (10 wt.% metal loading).

Metal particle size was measured from X-ray diffractometer. For all catalysts, the metal particle size was calculated by applying Scherrer's equation. The particle size of Pd, Pt, and Ni catalysts were 24.92 nm, 11.01 nm, and 5.64 nm, respectively. The large particle size of Pd/SiO_2 could enhance the adsorption of polyunsaturated FAMEs on the metal surface and also transform of *cis*-isomer to *trans*-isomer (Thunyaratchatanon 2012).

Table 4.4 Percentage of metal dispersion, particle size and Turnover Frequency (TOF)

Catalysts	Metal (111)	Particle size (nm) [a]	%Metal dispersion [b]	TOF (h^{-1})
Pd/SiO$_2$	Pd	24.97	14.00	3,958.93
Pt/SiO$_2$	Pt	11.01	7.42	1,856.80
Ni/SiO$_2$	Ni	5.64	5.60	233.04

[a] Particle size, measured by X-ray diffractometer.

[b] Metal dispersion, measured by CO pulse adsorption (Model R6015, Ohkura).

Figure 4.10 presents the XRD patterns of the 1 wt.% Pd/SiO$_2$ catalyst. For drying state, diffraction peaks were observed at 22.13° and 30.96°. These peaks corresponded to the peaks of Pd(NH$_3$)$_4$.Cl$_2$. In calcination state, the one main peak of metallic Pd and two main characteristic peaks of PdO according to the peaks at 41.05°, 60.20°, and 71.28°, respectively, were observed. After reduction state, PdO was reduced to metallic palladium. Diffraction peaks indicative of Pd were evident at 40.01° (1 1 1), 46.55° (2 0 0), and 68.20° (2 2 0), respectively. According to Numwong et al., 2012, the charaeteristic peaks of Pd including plane (1 1 1), (2 0 0), and (2 2 0) were found at 2Θ of 40.20°, 46.80°, and 68.25°, respectively.

Figure 4.11 shows the XRD patterns of Pt/SiO$_2$ catalyst. The broad peak at around 20° is due to diffraction by amorphous SiO$_2$ (Kaneko et al., 2012). In drying state, diffraction peaks were observed at 12.0°, 24.4°, and 27.2°. These peaks correspond to the peaks of Pt(NH$_3$)$_4$.Cl$_2$.H$_2$O. The catalyst calcined at 300 °C for 3 h, showed diffraction peaks of metallic Pt at 39.7° and 46.1°. This result was also confirmed by Ito et al., 2010. The Pt/SiO$_2$ catalyst reduced at 300 °C for 2 h also

showed the two main characteristic peaks of metallic Pt , 2Θ = 39.7° and 46.2°, which assigned to f.c.c. Pt(1 1 1) and Pt(2 0 0), respectively (McArdle *et al.*, 2010).

The X-ray diffraction patterns of 10 wt.% Ni/SiO_2 catalyst are shown in Figure 4.12. For drying state of Ni/SiO_2 catalyst, there is one main peak at 21.6°, which is the characteristic of SiO_2. The XRD pattern of the calcined catalyst showed peaks at 37.0°, 43.2°, and 62.8°, which are characteristics of NiO. Cruz *et al.*, 2011 and Park *et al.*, 2004 also found the NiO peaks observed at 2Θ = 37°, 43°, and 62°. After reduction state, NiO was reduced to metallic nickel. The XRD patterns of Ni was observed at 2Θ = 44.6°, 51.9°, and 76.2° (Sāraswat *et al.*, 2013 and Zhu *et al.*, 2011).
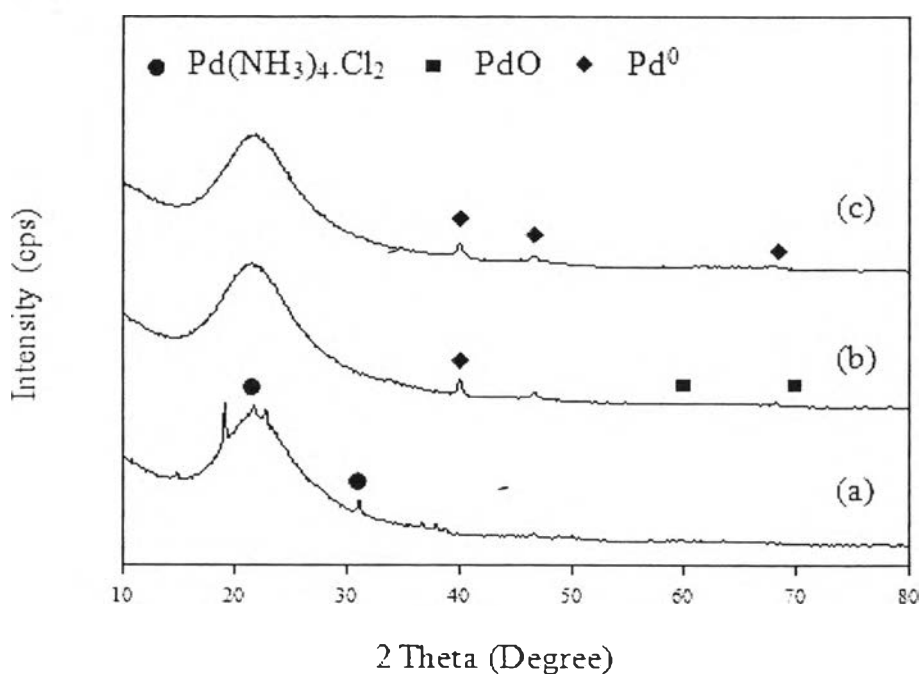
Figure 4.10 XRD patterns of 1 wt.% Pd supported on silica (a) dried, (b) calcined, and (c) reduced.
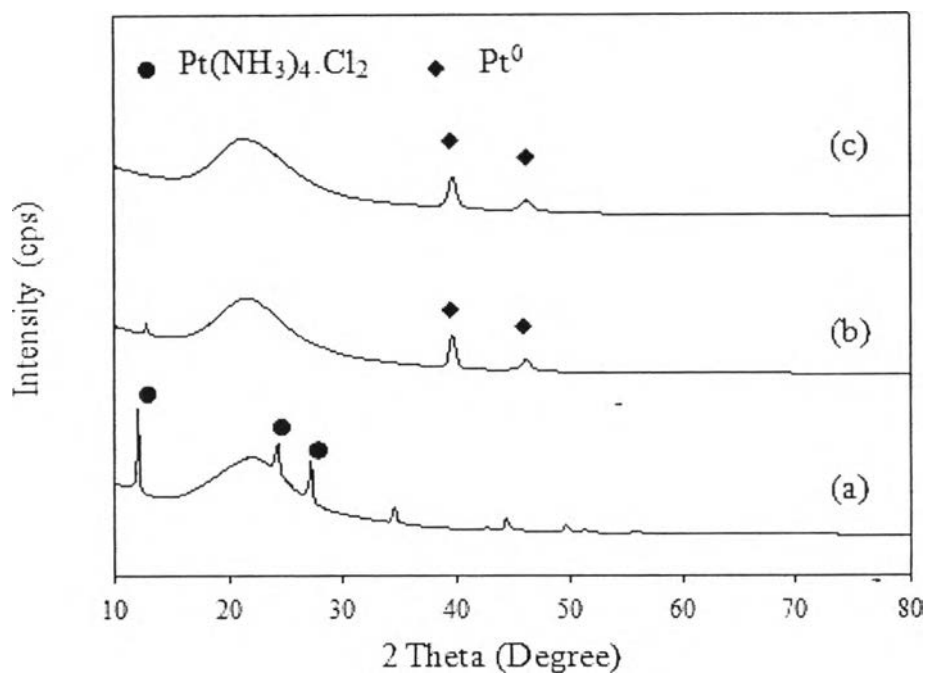
Figure 4.11 XRD patterns of 1.82 wt.% Pt supported on silica (a) dried, (b) calcined, and (c) reduced.
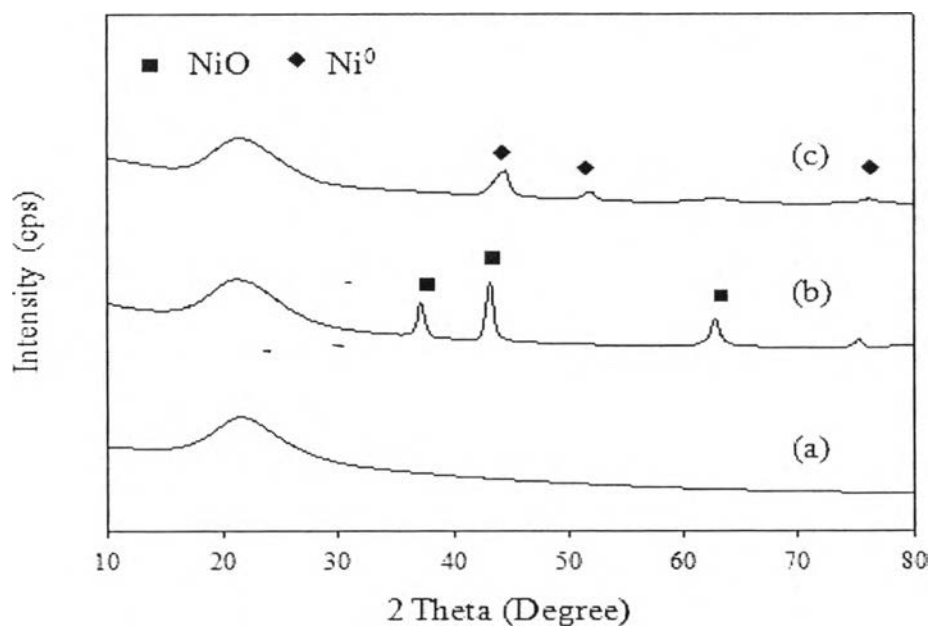
Figure 4.12 XRD patterns of 10 wt.% Ni supported on silica (a) dried, (b) calcined, and (c) reduced.

The BET surface area, total pore volume, and average pore diameter of SiO_2, Pd/SiO_2, Pt/SiO_2, and Ni/SiO_2, which were analyzed by using Autosorb-1 MP surface area analyzer are given in Table 4.5. It was found that, after Pd was impregnated on SiO_2 the BET surface area, total pore volume, and average pore diameter were slightly decreased as compared to the original support (SiO_2). It can be indicated that palladium was accessed in some pores of the support. For the Pt and Ni catalysts supported on SiO_2, they also presented the similar trend with Pd/SiO_2. Since the surface area of each catalyst just slightly change as compared to silica support. While both total pore volume and average pore diameter were decreased insignificantly that the results from some metal deposition in pores of support. Because of slight difference of surface properties between each catalyst, it can be suggested that these properties do not the significant factor for the catalytic activity.

Table 4.5 Surface area, total pore volume, and average pore diameter of SiO_2, Pd/SiO_2, Pt/SiO_2, and Ni/SiO_2 catalyst from Autosorb-1 MP surface area analyzer

| Catalyst	Surface area (m^2/g)	Total pore volume (ml/g)	Average pore diameter (nm)
SiO_2	112.50	1.27	45.17
Pd/SiO_2	109.80	1.19	43.34
Pt/SiO_2	110.00	1.20	43.46
Ni/SiO_2	112.40	1.11	39.31

4.3 Effect of Modifier on Partial Hydrogenation

The effect of magnesium-modifier on partial hydrogenation of soybean oil-based biodiesel was studied. The reaction was carried out on three types catalysts; Pd-Mg/SiO$_2$, Pt-Mg/SiO$_2$, and Ni-Mg/SiO$_2$, looking for a decrease in the *trans*-isomer formation during the partial hydrogenation reaction. The reaction were operated at 4 bar of hydrogen partial pressure, 80 °C, 150 ml/min of hydrogen flow rate, 1000 rpm of stirring rate, and 1 wt.% of the catalyst compared to 130.395 g of feed biodiesel (150 ml).

The FAMEs composition after partial hydrogenation reaction by using Pd-Mg/SiO$_2$ as a catalyst is shown in Figure 4.13(a). It exhibited that C18:3 and C18:2 dramatically decreased from 5.05% to 0.78% and 50.21% to 22.41%, respectively after 4 h of the reaction. The level of C18:0 increased from 3.89% to 4.60% after 4 h of the reaction. For *cis*-C18:1 and *trans*-C18:1 contents increased from 26.09% to 47.84% and 0.33% to 8.57%, respectively, at 4 h of the reaction time. For modified Pt catalyst, Pt-Mg/SiO$_2$, operated at 80 °C, the FAMEs composition is shown in Figure 4.13(b). It presented that C18:3 decreased from 5.09% to 2.98% and C18:2 decreased from 50.10% to 35.36%. While C18:0 slightly increased from 3.93% at starting time to 6.44% at the end of reaction time. The content of *cis*-C18:1 gradually increased from 26.07% to 38.14% after 4 h of the reaction. The *trans*-C18:1 content continually increased from 0.15% to 1.47% at 4 h of the reaction. And the last, partial hydrogenation reaction by using Ni-Mg/SiO$_2$ as a catalyst, the FAMEs composition is shown in Figure 4.13(c). The composition of C18:3 and C18:2 gradually decreased from 5.52% to 4.53% and 50.43% to 46.39%, respectively. The level of C18:0 increased from 3.62% to 4.16% after 4 h of the reaction. While *cis*-C18:1 slightly increased from 25.72% to 28.28%. The *trans*-C18:1 content slightly increased from 0.28% to final values at 0.96% after 4 h of reaction.

An interesting observation is an increase of both C18:0 and *cis*-C18:1 composition with the time on stream, the *trans*-C18:1 content decreases with the addition of magnesium modifier, as presented in Figure 4.11. This result agrees well

with the work of Tonetto and co-workers. This caused a block of part of the surface by the modifiers (Tonetto *et al.*, 2009).
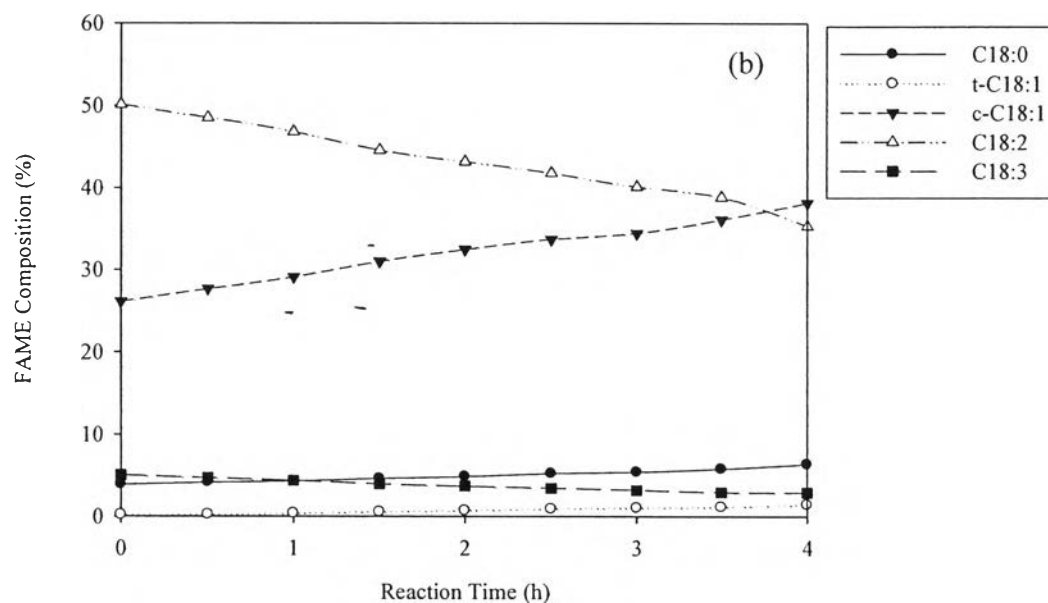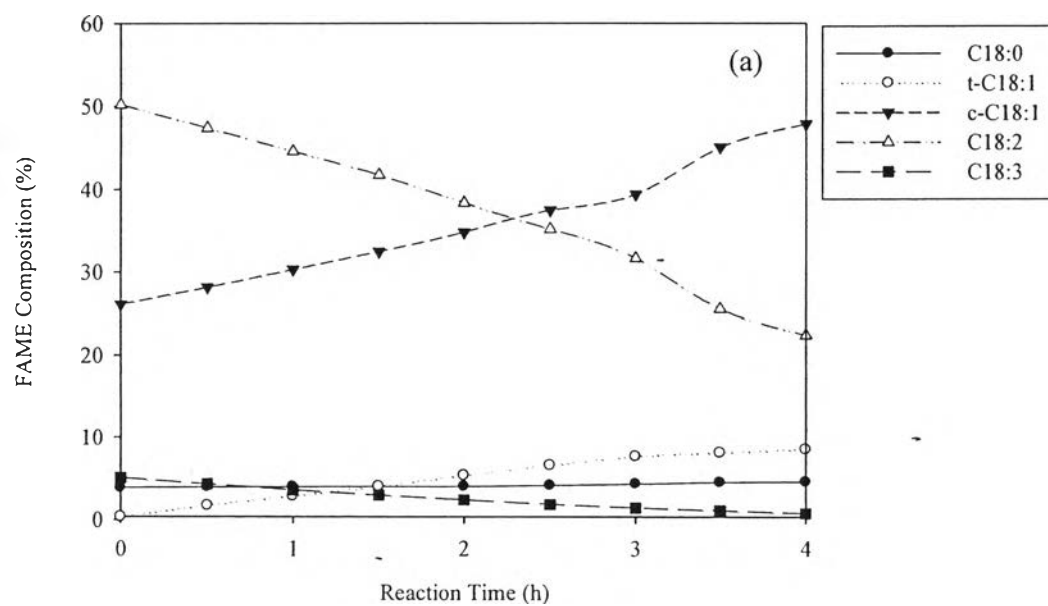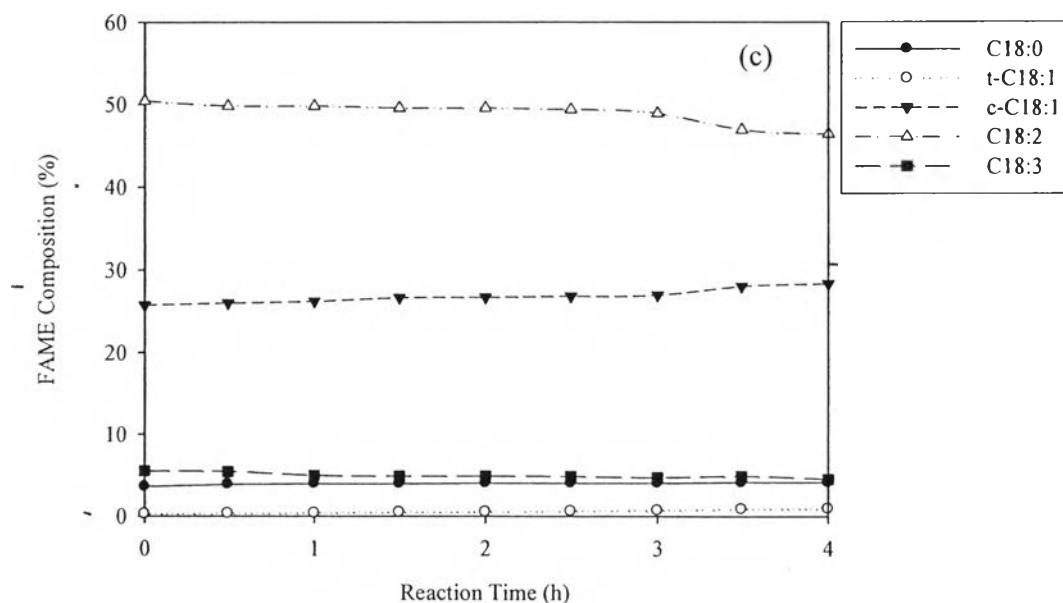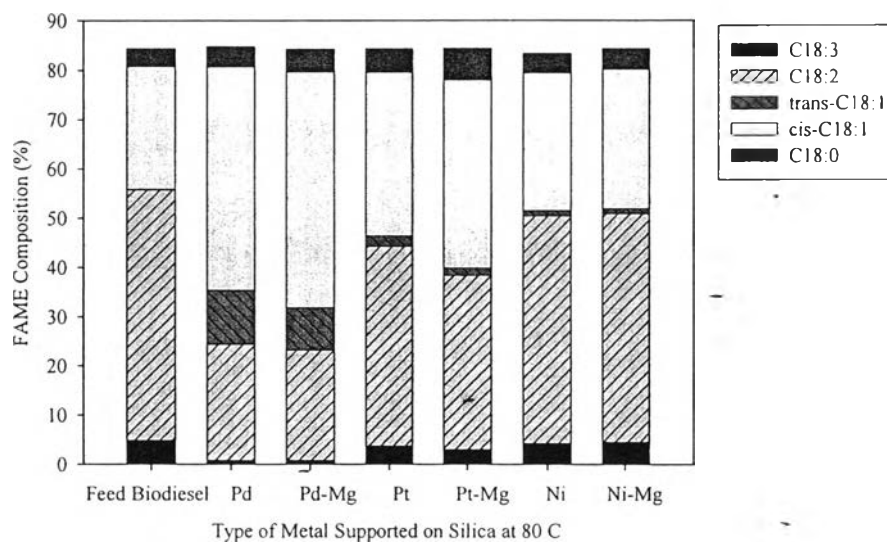
Figure 4.13 Effect of modifier of biodiesel after hydrogenation reaction (4 h) in conditions : 80 °C, 4 bar, 150 ml/min of H_2 flow rate, 1000 rpm of stirring rate, 1 wt.% of Pd-Mg loading, 1.82 wt.% of Pt-Mg loading, 10 wt.% of Ni-Mg loading and 1 wt.% of catalyst.

From the results shown in Figure 4.14 and Table 4.6, it evidently showed that a lower *trans*-C18:1 content was observed for all catalysts. For Pd-Mg/SiO$_2$ catalyst, *trans*-C18:1 of 8.57% was obtained, when compared to that of Pd/SiO$_2$ catalyst (10.57%). The percentage decrease in *trans* content was 21.74%. For the Pt catalyst, *trans* content dropped from 2.13% to 1.47% (a drop of 30.99%), while the Ni catalyst slightly decreased *trans* content from 1.08% to 0.96% (a drop of 11.11%).

Therefore, it can be concluded that a decrease of the *trans*-C18:1 formation was also observed for magnesium modified catalysts on the partial hydrogenation of soybean oil. This result is consistent with the work done by Tonetto and co-workers. They found that *trans*-isomer decreases with the addition of the magnesium modifier. The results can be interpreted in terms of different effects: change in the electron density of metals, which affects the relative adsorption strength of the reactant, intermediates and hydrogen, and a block of part of the surface by the modifiers.

Figure 4.14 Comparison of C18 FAME composition of biodiesel after hydrogenation reaction (4 h) in conditions : 80 °C, 4 bar, 150 ml/min of H_2 flow rate, 1000 rpm of stirring rate, 1 wt.% of Pd loading, 1 wt.% of Pd-Mg loading, 1.82 wt.% of Pt loading, 1.82 wt.% of Pt-Mg loading, 10 wt.% of Ni loading, 10 wt.% of Ni-Mg loading and 1 wt.% of catalyst. -

Table 4.6 *Trans*-C18:1 content after hydrogenation reaction (4 h) of soybean oil: (reaction conditions: 80 °C, 4 bar, 150 ml/min of H_2 flow rate, 1000 rpm of stirring rate, 1 wt.% catalyst

| Catalytic System	*Trans*-C18:1 (%)	Reduction of *Trans*-C18:1 (%)
Pd/SiO₂	10.95	
Pd-Mg/SiO₂	8.57	21.74
Pt/SiO₂	2.13	
Pt-Mg/SiO₂	1.47	30.99
Ni/SiO₂	1.08	
Ni-Mg/SiO₂	0.96	11.11

The XRD patterns of Pd-Mg/SiO$_2$ catalyst are shown in Figure 4.15. The X-ray diffraction pattern of the dried catalyst showed peaks at 30.96°, which is characteristics of Pd(NH$_3$)$_4$.Cl$_2$. The catalyst calcined at 300 °C for 3 h, showed one diffraction peak of metallic Pd and two diffraction peaks of PdO at 41.05°, 60.20°, and 71.28°, respectively. After calcinations state, the palladium phase in Pd-Mg/SiO$_2$ was also observed to be PdO at 60.12° and 71.41°, and the absence of reflections for the magnesium phase (Park et al.,2009). After reduction state, the XRD patterns were changed from calcinations which meant that PdO was changed to be metallic Pd at 2Θ of 40.01° and 46.55° (Numwong et al., 2012).

The XRD patterns of Pt-Mg/SiO$_2$ catalyst are shown in Figure 4.16. For drying state of Pt/SiO$_2$ catalyst, there are three main peaks at 12.0°, 24.4°, and 27.2°. These peaks indicated to Pt(NH$_3$)$_4$.Cl$_2$. The XRD pattern of the calcined catalyst showed peaks at 39.79° and 46.17°, which are characteristics of metallic Pt. The dried Pt-Mg/SiO$_2$ catalyst showed two diffraction peaks of metallic Pt at 39.64°, and 46.07°, respectively. The Pt-Mg/SiO$_2$ catalyst calcined at 500 °C for 4 h showed the two main characteristic peaks of metallic Pt at 2Θ = 39.74° and 46.08°. Whereas, the XRD patterns of magnesium phase were not found. This implies that magnesium was highly dispersed on catalyst surface (Zhu et al., 2011). After reduction state, diffraction peaks were observed at 39.74° and 45.99°. These peaks correspond to the peaks of metallic Pt (McArdle et al., 2010).

The XRD patterns of Ni-Mg/SiO$_2$ catalyst are shown in Figure 4.17. In drying state, there was one main peak at 21.60°, contributed to SiO$_2$. The X-ray diffraction pattern of the calcined catalyst showed peaks at 43.09° and 62.77° which are characteristics of NiO, also showed the two main characteristic peaks of Ni at 75.48° and 79.36°. The Ni-Mg/SiO$_2$ catalyst dried at room temperature and 60 °C, showed two diffraction peaks of NiO and two diffraction peaks of metallic nickel at 43.11°, 62.78°, 75.43°, and 79.38°, respectively. After calcinations state, the XRD patterns showed peaks at 43.26° and 62.79°, suggesting that NiO. In addition, the XRD patterns showed two main peaks of Ni at 75.34° and 79.35°. The pattern absence of reflection for the magnesium phase. The XRD pattern of the reduced catalyst showed peaks at 74.47° and 79.30°, which are characteristics of metallic Ni.
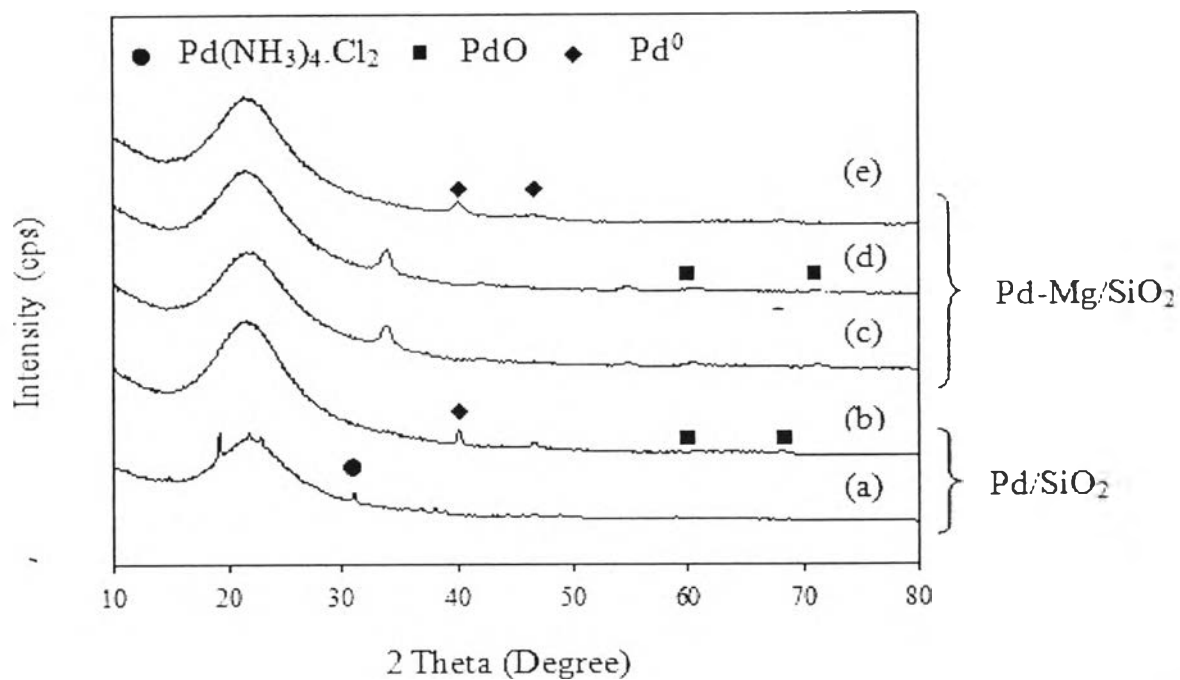
Figure 4.15 XRD patterns of Pd supported on silica (a) dried, (b) calcined, Pd-Mg supported on silica (c) dried, (d) calcined, and (e) reduced.
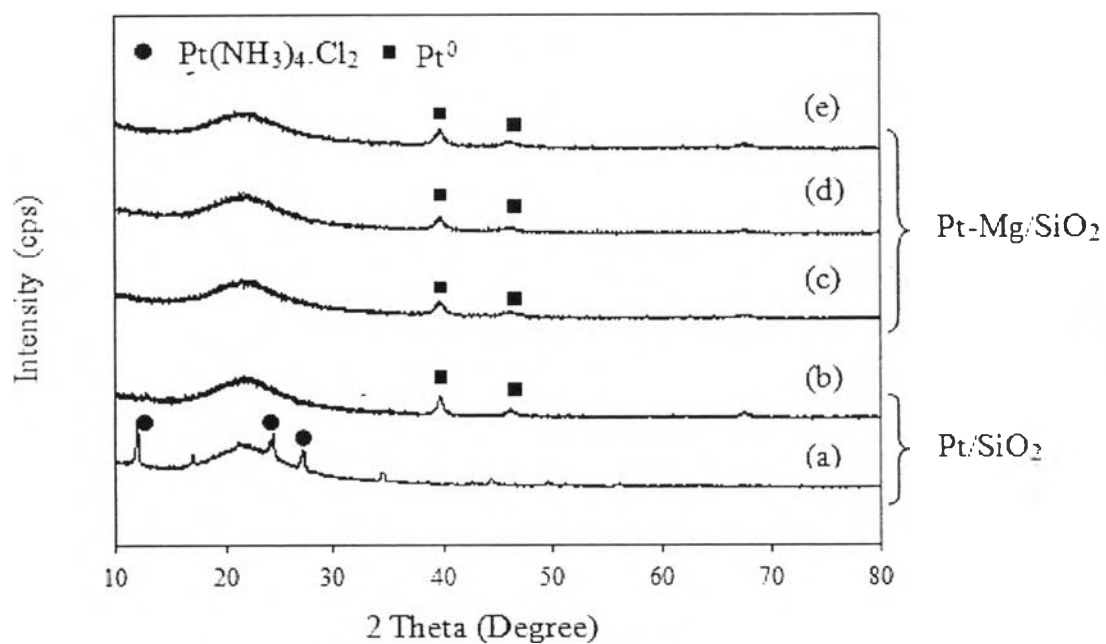
Figure 4.16 XRD patterns of Pt supported on silica (a) dried, (b) calcined, Pt-Mg supported on silica (c) dried, (d) calcined, and (e) reduced.
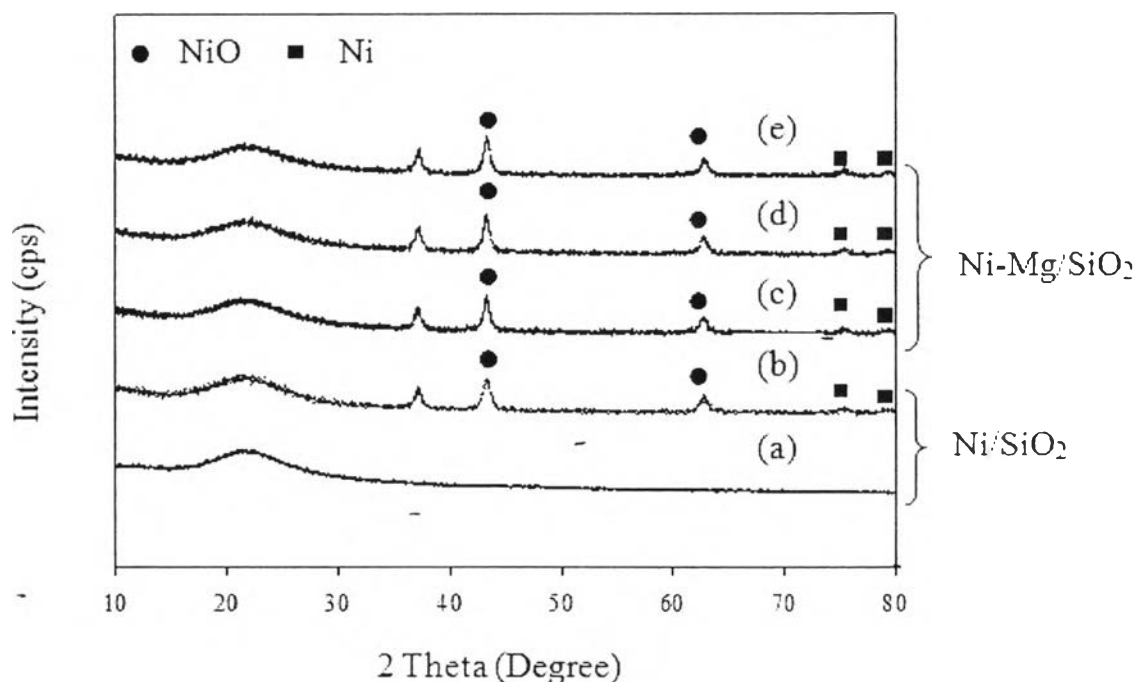
Figure 4.17 XRD patterns of Ni supported on silica (a) dried, (b) calcined, Ni-Mg supported on silica (c) dried, (d) calcined, and (e) reduced.

The BET surface area, total pore volume, and average pore diameter of Pd/SiO_2, Pt/SiO_2, Ni/SiO_2, $Pd-Mg/SiO_2$, $Pt-Mg/SiO_2$, and $Ni-Mg/SiO_2$, which were analyzed by using Autosorb-1 MP surface area analyzer are given in Table 4.7. For $Pd-Mg/SiO_2$ and $Pt-Mg/SiO_2$ catalysts, the BET surface area was slightly increased. It can be suggested that Pd-Mg mefals and Pt-Mg metals were deposited on some pores of the support. For Ni-Mg was impregnated on SiO_2 the BET surface area was slightly decreased as compared to the Ni/SiO_2. It can be indicated that Ni-Mg was accessed in some pores of the support. However, their surface area and pore diameter do not shows a strong relation between physical property and catalytic activity for partial hydrogenation of biodiesel. In addition, the interaction between MgO and SiO_2 could also have a positive influence in support catalysts by decreasing the amount of non-selective sites (MgO) (Solsona *et al.*, 2001).

Table 4.7 Surface area, total pore volume, and average pore diameter of Pd/SiO$_2$, Pt/SiO$_2$, Ni/SiO$_2$, Pd-Mg/SiO$_2$, Pt-Mg/SiO$_2$, and Ni-Mg/SiO$_2$ catalyst from Autosorb-1 MP surface area analyzer

Catalyst	Surface area (m^2/g)	Total pore volume (ml/g)	Average pore diameter (nm)
Pd/SiO$_2$	109.80	1.19	43.34
Pd-Mg/SiO$_2$	114.40	1.23	43.10
Pt/SiO$_2$	110.00	1.20	43.46
Pt-Mg/SiO$_2$	114.10	1.24	43.29
Ni/SiO$_2$	112.40	1.11	39.31
Ni-Mg/SiO$_2$	107.30	1.06	39.52

4.4 Biodiesel Properties

The oxidative stability, cloud point, and cold filter plugging point of feed biodiesel and hydrogenated FAMEs were investigated as presented in Table 4.8. It apparently shows that hydrogenated biodiesel product after 4 h of reaction time for all catalysts gave higher oxidative stability. This result is in accordance with the work done by Numwong and co-workers. They found that the composition of polyunsaturated FAMEs (C18:2 and C18:3) as a function of oxidative stability. After hydrogenation; the composition of C18:2 and C18:3 decreased with an improvement of oxidative stability. The longer hydrogenation time, the lower composition of C18:2 and C18:3, and the higher oxidative stability are observed. Moreover, could point and cold filter plugging point were increased which the result from increasing amount of C18:0 in hydrogenated biodiesel. However, oxidative stability and cold filter plugging point of hydrogenated biodiesel with adding Mg modifier were higher than that of without adding Mg modifier.

Therefore, it can be concluded that the partial hydrogenation reaction can improve the biodiesel properties especially oxidative stability. This was supported by a decrease of amount of C18:2 and C18:3 (Thunyaratchatanon, 2012). In addition, the greater amount of C18:0, results in an increase in cold flow properties. (Numwong et al., 2012).

Table 4.8 Biodiesel properties before and after partial hydrogenation

Catalyst	Oxidative Stability (h)	Cloud point (°C)	Cold Filter Plugging Point (°C)
Feed Biodiesel	2	7	-6
Pd/SiO₂			
• 120 °C	6.2	10	-4
• 100 °C	7.3	8	-3
• 80 °C	10.4	10	-3
• Pd-Mg/SiO₂ at 80 °C	11	10	-2
Pt/SiO₂			
• 120 °C	4	12	-2
• 100 °C	4.7	12	-4
• 80 °C	4.8	13	-4
• Pt-Mg/SiO₂ at 80 °C	5.4	12	-2
Ni/SiO₂			
• 120 °C	3	9	-2
• 100 °C	2.6	13	-5
• 80 °C	2.7	12	-5
• Ni-Mg/SiO₂ at 80 °C	3.5	12	-1